A Study on the Aerodynamic Properties of the NACA 0015 Airfoil Using Wind Tunnel Experiment

Saad Jabbar Nghaimesh

saad.nghaimesh@stu.edu.iq
Southern Technical University/ Al-Nasiriyah Technical Institute/Mechanical Technology Department

ABSTRACT

The NACA 0015 airfoil model underwent wind tunnel testing using the Educational Wind Tunnel-PC Linked Three Component Balance (WT300). The primary objective of the experiment was to assess the airfoil's aerodynamic characteristics at constant velocities of 20m/s and 30m/s across Angles of Attack (AOA) with a vast variety, ranging from 0 degrees to 35 degrees AOA. The wind tunnel's three-component balance directly measured the drag and lift forces. Analysis of the data revealed Cl (coefficient of lift) and Cd (coefficient of drag) values of approximately -0.7 and 0.9, respectively. Comparing the two speeds, the lift-to-drag ratio was higher at 20m/s compared to 30m/s. Additionally, the coefficient of lift at 20m/s was greater than that at 30m/s. Rather than using smoke visualization, the tuft flow technique was employed in this experiment, which involves attaching filaments or strings at various positions on the model for flow visualization. The results indicated that stalling occurred for the NACA 0015 airfoil at an AOA range between $20° < \alpha \leq 30°$ when the speed was set at 30m/s, while at 20m/s, stalling occurred at 15° within the AOA range of $10° < \alpha < 20°$.

Keywords: Wind Tunnel, Flow Visualization, Theory of Flight

1. Introduction

1.1 Theory of Flight

The Theory of Flight is commonly explained using Bernoulli's Equation, which states energy conservation as a principle. The air's energy must always remain constant, but according to Bernoulli's Principle, air going over the top of an aerofoil or wing must move farther and hence more quickly than air moving beneath the wing at the same time. Since the atmosphere above and below the has differing pressures, the lift is created by this pressure difference. Equation (1) shows that dynamic pressure, surface area, and lift coefficient are all characteristics of the lift.

$$L = 1/2\ \rho V^2 A_S\ C_L \quad (1)$$

According to Equation (2), drag is a function of dynamic pressure, surface area, and drag coefficient.

$$D = 1/2\ \rho V^2\ A_S\ C_D \quad (2)$$

Equation (3) displays dynamic pressure.

$$p_d = 1/2\ \rho V^2 \quad (3)$$

Equation (4) illustrates the relationship between Surface Area (As) and the chord and span.

$$AS = cl \quad (4)$$

Equation (5) illustrates Bernoulli's equation as a function of pressure, density, velocity, and specific weight.

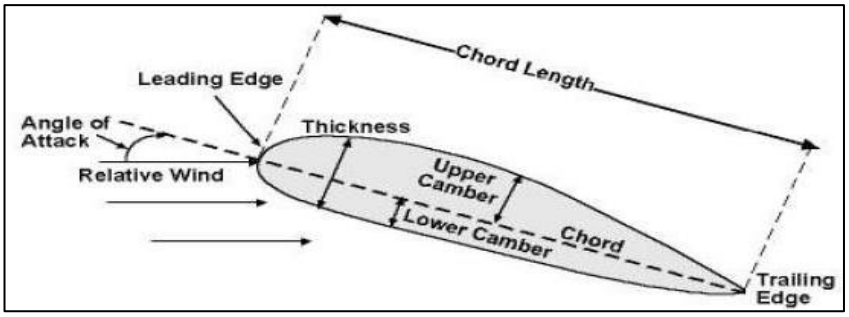

Figure 1. Airfoil Nomenclature.

$$\frac{P_1}{\rho g} + \frac{{V_1}^2}{2g} + Z_1 = \frac{P_2}{\rho g} + \frac{{V_2}^2}{2g} + Z_2 \quad (5)$$

The equation can be written as Equation (6), which can then be rearranged to become Equation (7), which represents the streamline's velocity, presuming Z1=Z2, or that the heights are at the same level.

$$\frac{P_2 - P_1}{\rho g} = \frac{{V_1}^2}{2g} \quad (6)$$

$$V = \sqrt{2gh} \quad (7)$$

Although the wind tunnel use fluid (air) and uses water as a medium for measurement, equation (7) above is ideal for water-based activities like running with water and measuring with water. It is necessary to include Air Density in the equation to use it. As a result, the conversion factor (Equation (8)) must be included in Equation (7) before it can be rearranged into Equation (9) for use in determining the velocity in this experiment.

$$\text{Conversion Factor} = \frac{\rho_{water}}{\rho_{air}} \quad (8)$$

$$V = \left(\sqrt{2gh}\right) x \frac{\rho_{water}}{\rho_{air}} \quad (9)$$

1.2 NACA 0015 Airfoil

An airfoil is a cross-sectional shape formed when a wing intersects with a perpendicular plane. When an airfoil travels through the air, the air is broken up into two portions and passes above and below the wing because of its streamlined shape or profile. The framing of the wing's upper surface allows the air rushing over it to reach and extend [1]. Due to the stream's preoccupation with the bottom side, as seen in Figure 1 [2], the flow is accelerated across the aerofoil. Close to the suction crest area, a higher mean speed is seen [3,4]. The angle of maximum lift can be significantly increased when an airfoil is quickly shifted over an AOA range that includes the static stall angle [5]. In addition, the Lift force increases with a higher angle of attack up to a critical angle. Beyond this critical angle, the lift force decreases significantly and the wing is said to have “stalled”. The NACA 4-digit series of airfoil categorization includes the NACA 0015 airfoil. The four digits are established by the airfoil's properties in the manner shown below [6]. The maximum camber is expressed as a percentage of the chord in the first digit. The second digit indicates the percent of the chord where the chord's highest camber is located when measured from the leading edge. The airfoil's maximum percent chord thickness is indicated by the last two digits. As a result, the NACA 0015 airfoil is symmetrical and cambered-free.

1.3 Wind Tunnel

The wind tunnel is a piece of equipment that creates a controlled stream of air to research how aircraft models and other machinery and things react to air resistance or movement. Plastrochem Co. Ltd.'s Educational Wind Tunnel-PC Linked Three Component Balance (WT300) was used in this investigation. A good technique to study aerodynamics is with this computer-linked wind tunnel equipment. By using three-component balancing, drag and lift forces may be quantified directly. The computer screen will display the air temperature and velocity, which are also directly read. When

utilizing appropriate software and hardware that is compatible with the Windows program on a computer, the results of experiments on various models, like an automobile, aerofoil, and wing, may be calculated and displayed on the screen. The technical requirements are listed below [7].

Figure 2. Wind Tunnel WT300 Technical prerequisites.

1. Dimension: Test Section, approximately (300 mm x 300 mm x 900 mm). 1065 mm2 entrance cone with a 12:1 contraction ratio. (4.4) m in total length.
2. The weight is 400 kg.
3. The volume is 10 m3.
4. Variable air velocity of up to 46 m/s with no load
5. Construction Substances: With four wheels and eight locking wheels, the frame is made of mild steel. Galvanized steel sheet is the inlet cone. There is a diffuser for the air. Galvanized steel sheet, smooth inner surface; tailpipe.
6. Blower: Provided with frequency inverter 0-60 Hz, fan guard, and silencer. Axial type, high speed, powerful > 10 HP motor.
7. Three Component Balance: solid frame type; model supporter may rotate 360 degrees; forces are detected by load cells with an A/D converter and the software required to link with a computer; maximum capacities are for the lift of 50N and drag of 25N.
8. The Angle-Feedback Unit is intended to be put on a two-component balance and used to measure the angular position of models with a 0.1-degree resolution.
9. S-type Pitot tube with an inclined manometer for airspeeds greater than 20 m/sec.
10.PowerSupply: 3 phase, 50 Hz, 380-415 VAC, 15 amp.

2. Experimental Setup

setups were done. There are the calibration setup and experiment setups.

2.1 Calibration

Insert the Pitot tube into the centre position of the test area and connect the vinyl tube from the Pitot tube to the manometer.

2.2 Experiment

1. The airfoil model NACA 0015 (figure 3a) is mounted by inserting its hole into the stick-out axle as shown in figures (3b) and c that connects to 3 component balance unit at the test section area.
2. Next, lock the screw by tightening 3 screws with a hexagon wrench.
3. Then, the test section is closed to avoid any loss which can affect the experiment.

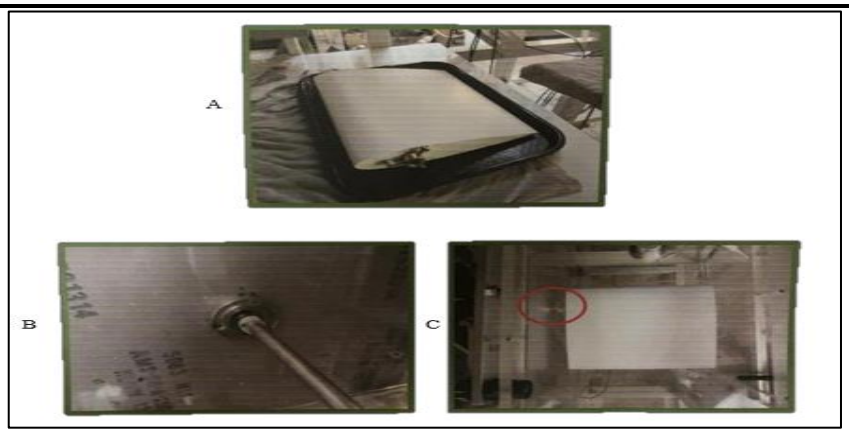

Figure 3. NACA 0015 airfoil setup (a) NACA 0015 Airfoil (b) stick out the axle (c) Top view of the test area

3. Procedure

3.1 Calibration

- The wind tunnel is switched on. The wind tunnel is let to run for a few minutes before it can be used for the experiment by adjusting the fan rotational frequency.
- The frequency of the fan is regulated incrementally from 5 Hz to 10 Hz with an interval of 1 Hz.
- Then the frequency of the fan is regulated incrementally from 10 Hz to 45 Hz with an interval of 5 Hz.
- Then, the height difference of the manometer is recorded and tabulated on the spreadsheet with the frequency of the fan.
- The velocity of the wind is calculated based on Equation (9).
- The wind tunnel is then switched off after the process is completed.

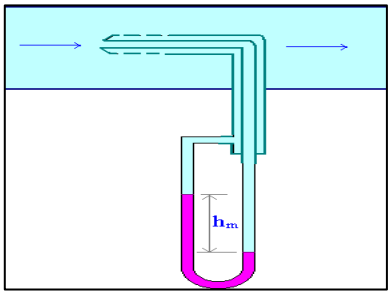

Figure 4. Schematic Diagram of Pitot tube with Manometer.

3.2 Flow Visualization

Flow visualization enables the person outside of the test area to view the flow of the air around the Airfoil. Typically, a smoke visualization technique is used whereby a smoke generator generates a desired amount of smoke sufficient to visualize the flow of air around an airfoil. Depending on the needs of the experiment, a dye is used to produce colored smoke. In this experiment, the smoke visualization technique can't be used as the smoke generator of the wind tunnel is under maintenance. So, the next option is using the tuft flow technique. This method uses a filament or string that is attached to the model in one, many, or many locations. Tufts resemble grass blades that are blowing in the wind, and many tuft installations incorporate a dye or luminous covering that makes it possible to detect movement in ordinary light.

3.3 Experiment

1. The wind tunnel is then switched on.
2. The wind tunnel is let to run for a few minutes before it can be used for the experiment by adjusting the fan speed frequency.

3. The Wind Tunnel software is opened and keyed in data (temperature, velocity, angle of attack, chord, and wing length) before the experiment can proceed.
4. Airspeed is adjusted by rotating the frequency roller switch.
5. The angle of attack of (0°) is set with the fixed velocity of airspeed (20 m/s).
6. Then, the details (coefficient of drag and lift, drag and lift force) are then recorded through the wind tunnel software.
7. The process is then repeated for the angle of attack (5°,10°,15°, 20°, 25°, 30°)
8. After the process of various(AoA) with fixed velocity is completed, the velocity of 30 m/s is then used for the next experiment with the same process 7.
9. The wind tunnel is then switched off after the process is completed.

4. DATA

4.1 Calibration

Initially, the speed control chart table was given by manufacturing as below (Table 1). Then, using a pitot-static tube and an inclined manometer, readings of a pressure gradient were used to create the calibrated speed control chart. (Table 2) and calculated by using Equation (9).

Table 1: Manufacturing Speed Control Chart.

Frequency (Hz)	V, m/s
5	5.2
6	6.5
7	7.4
8	8.4
9	9.5
10	10.6
15	15.4
20	20.5
25	25.5
30	30.5
35	35.5
40	40.5
45	45.5

Table 2: Pitot Tube Speed Control Chart.

Frequency, Hz	Pitot Tube	
	h, cm	V, m/s
5	0.1	4.07
6	0.15	4.98
7	0.2	5.75
8	0.3	7.05
9	0.4	8.14
10	0.5	9.10
15	1.5	15.75
20	2.9	21.91
25	5.1	29.05
30	7.6	35.46
35	10.4	41.48
40	13.7	47.61
45	17.2	53.35

Figure 5 shows that the velocity has been fitted linearly concerning frequency. Using Equation (10), the velocity for any chosen frequency can be computed.

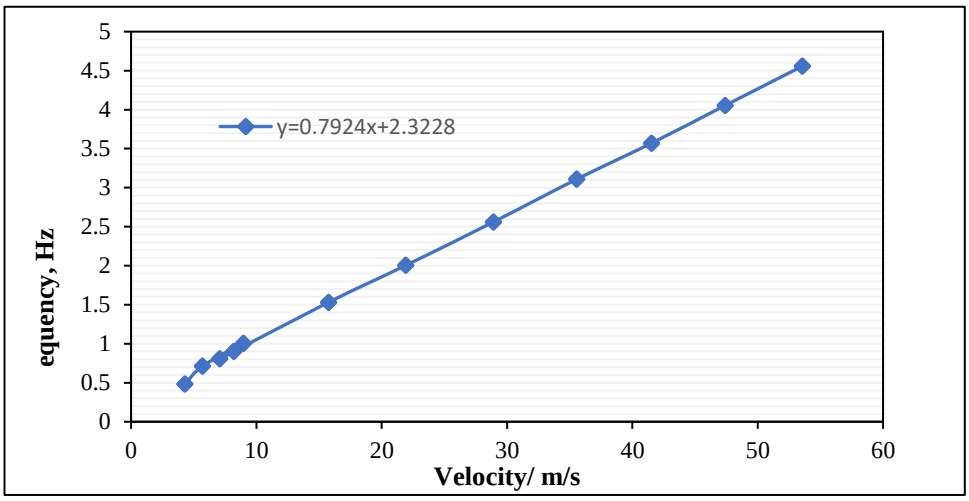

Figure 5. Calibrated Frequency Vs Velocity Graph.

From the linear fitted graph for Velocity Vs Frequency above, the generated equation is as below:

$$y = 0.7924xr + 2.3228 \quad (10)$$

Where y = Frequency, Hz x = Velocity, m/s

For this experiment, since we are using 20m/s & 30m/s airspeed, the frequency selected yield from Equation 10 is 18.2 Hz and 26.1 Hz respectively. To determine the r2 or coefficient of determination for this calibration, the equation below was used:

$$r^2 = 1 - \frac{SE_{line}}{SE_y} \quad (11)$$

Where the SE_{line} is Squared Error between the point and line is computed by using the equation below:

$$\Sigma (y_1 - (mx_1 + c))^2 + (y_2 - (mx_2))^2 ..... + (mx_n + c))^2 \quad (12)$$

Where m and c values in this calculation obtained above 0.7924 and 2.3228 respectively

SE_y is the Total Variation in y computed by using the equation below:

$$\Sigma (y_1 - y_{avg})^2 + (y_2 - y_{avg})^2 .... + (y_n - y_{avg})^2 \quad (13)$$

Table 3: Squared Error Analysis

Frequency (y)	Velocity (x)	SE line	SE_y
5	4.07	0.2983	213.6095
6	4.98	0.0732	185.3787
7	5.75	0.0141	159.1479
8	7.05	0.0089	134.9172
9	8.14	0.0531	112.6864
10	9.10	0.2205	92.4556
15	15.75	0.0373	21.3018
20	21.91	0.1017	0.1479
25	29.05	0.1170	28.9941
30	35.46	0.1791	107.8402
35	41.48	0.0379	236.6864
40	47.61	0.0026	415.5325
45	53.35	0.1628	644.3787
TOTAL		1.3066	2353.0769

Hence,

$$r^2 = 1 - \frac{1.3066}{2353.0769} = 0.9994$$

The r2 result above shows that the r2 value is close to 1, which tells us that a lot of variation in the y-axis is described by the variation in x. Therefore, the line is a good fit.

4. 2 Experiment

According to the experiment procedure stated above (4.2), the measurement data is recorded as below:

For a constant speed of 20 m/s.

Table 4. Lift and drag (vs) angle of attracting 20m/s.

Angle of attack	force (N).	
	lift	drag
0	0.02	-0.49
5	-0.126	-1.374
10	-0.192	-1.498
15	-1.304	0.094
20	-0.448	-1.672
25	-0.372	-1.268
30	0.828	-0.366

For a constant speed of 30 m/s.

Table 5. Lift & Drag vs Angle of Attack (30 m/s).

Angle of Attack	Force (N)	
	Lift	Drag
0	1.98	-3.23
5	0.538	-3.09
10	0.916	-1.404
15	4.562	0.324
20	3.916	1.758
25	4.362	1.668
30	5.102	1.062

5. Uncertainty

5.1 Uncertainty Analysis on Pitot Tube

The uncertainty in the velocity of the air obtained from the Pitot tube was calculated using Equation 14 below:

$$\frac{\Delta v}{v} = \sqrt{\frac{1}{2}(\frac{\Delta h_L}{h_l})^2 + (\frac{\Delta h_R}{h_R})^2}$$

Table 6: Uncertainty Calculation Table for Coefficient of CL.

h_L	Δh_L	h_g	Δh_R	Velocity V	ΔV
8.9	0.005	8.8	0.005	4.07	0.0023
8.9	0.005	8.75	0.005	4.98	0.0028
9	0.005	8.8	0.005	5.75	0.0032
9.35	0.005	9.05	0.005	7.05	0.0038
10.3	0.005	9.9	0.005	8.14	0.0040
11.35	0.005	10.85	0.005	9.10	0.0041
12.6	0.005	11.1	0.005	15.75	0.0067
14.1	0.005	11.2	0.005	21.91	0.0088
12.7	0.005	7.6	0.005	29.05	0.0157
10.1	0.005	7.6	0.005	35.46	0.0206
16	0.005	5.6	0.005	41.48	0.0277

17	0.005	3.3	0.005	47.61	0.0520
18.5	0.005	1.3	0.005	53.35	0.1454

Hence, the average value on Δs is 0.022876 m/s.

5.2 Uncertainty Analysis on FL

The experiment was conducted by using two velocities (20 m/s and 30 m/s) for different 7 angles of attack and the uncertainty in the lift force is found using Equation 15 below:

$$\Delta FL = \sqrt{(2 \text{ X Std Dev } (FL))2 + 0.12}$$

Table 7: Lift force uncertainty calculation for 20 m/s.

The angle of Attack (°)	F_L	(F_L - Average F_L)	(F_L - Average F_L)^2
0	0.0200	0.2477	0.0614
5	-0.1260	0.1017	0.0103
10	-0.1920	0.0357	0.0013
15	-1.3040	-1.0763	1.1584
20	-0.4480	-0.2203	0.0485
25	-0.3720	-0.1443	0.0208
30	0.8280	1.0557	1.1145
Average FL	-0.2277	$\sum$ (f***L*** – **Average *FL*)2**	0.3450

Hence, Std Dev (FL) = 0.6345

$\Delta FL = \sqrt{(2 \text{ X } 0.6345)^2 + 0.1^2}$ =1.2729

Hence, ΔFL is calculated to be 1.2729 N for 20 m/s.

Table 8: Lift force uncertainty calculation for 30 m/s.

The angle of Attack (°)	F_L	(F_L - Average F_L)	(F_L - Average F_L)^2
0	1.9800	-1.0737	1.1529
5	0.5380	-2.5157	6.3288
10	0.9160	-2.1377	4.5698
15	4.5620	1.5083	2.2749
20	3.9160	0.8623	0.7435
25	4.3620	1.3083	1.7116
30	5.1020	2.0483	4.1955
Average FL	3.0537	$\sum$ (F***L*** – **Average *FL*)2**	20.9771

Hence, Std Dev (FL) = 1.8698

$\Delta FL = \sqrt{(2 \text{ X } 1.8698)^2 + 0.1^2}$ = 3.740

Hence, ΔFL is calculated to be 3.7409 N for 30 m/s.

5.3 Uncertainty Analysis on CL

The uncertainty in the coefficient of lift was calculated using Equation 16 below:

$$\Delta C_L = \sqrt{(\frac{\Delta E_L}{F_L})^2 + (-2\Delta V)^2}$$

Where ΔFL for 30 m/s = 3.7409 N and 20 m/s = 1.2729 N and ΔV = 0.022876 m/s is obtained based on the calculation above.

Table 9: Coefficient of Lift uncertainty calculation for 20 m/s.

The angle of Attack (°)	F_L	ΔC_L
0	0.0200	63.6429
5	-0.1260	10.1022
10	-0.1920	6.6296
15	-1.3040	0.9772
20	-0.4480	2.8416
25	-0.3720	3.4220
30	0.8280	1.5379
Average ΔC_L		12.7362

Hence, the average value on ΔCL for 20 m/s is calculated to be 12.7362.

Table 10: Coefficient of Lift uncertainty calculation for 30 m/s.

The angle of Attack (°)	F_L	ΔC_L
0	1.9800	1.8899
5	0.5380	6.9536
10	0.9160	4.0843
15	4.5620	0.8213
20	3.9160	0.9564
25	4.3620	0.8588
30	5.1020	0.7347
Average ΔC_L		2.1175

Hence, the average value on ΔCLfor 30 m/s is calculated to be 2.1175.

5.4 Uncertainty Analysis on FD.

The experiment was conducted by using two velocities (20 m/s and 30 m/s) for different 7 angles of attack and the uncertainty in the drag force is found using Equation 17 below:

$$\Delta FD = \sqrt{\left(2X\ Std\ Dev\ (FD)\right)2 + 0.12}$$

Table 11: Force of Drag uncertainty calculation for 20 m/s.

The angle of Attack (°)	F_D	(F_D - Average F_D)	(F_D - Average F_D)^2
0	-0.4900	0.4491	0.2017
5	-1.3740	-0.4349	0.1891
10	-1.4980	-0.5589	0.3123
15	0.0940	1.0331	1.0674
20	-1.6720	-0.7329	0.5371

25	-1.2680	-0.3289	0.1081
30	-0.3660	0.5731	0.3285
Average F_D	-0.9391	$\sum (F_D - \textbf{Average } F_D)^2$	2.7443

Hence, Std Dev (FD) = 0.6763

$\Delta FD=\sqrt{(2 * 0.6763)2 + 0.12}=1.3563$

Hence, ΔFD is calculated to be 1.3563 N for 20 m/s.

Table 12: Force of Drag uncertainty calculation for 30 m/s

The angle of Attack (°)	FD	(FD - Average FD)	(FD - Average FD)2
0	-3.2300	-2.8140	7.9186
5	-3.0900	-2.6740	7.1503
10	-1.4040	-0.9880	0.9761
15	0.3240	0.7400	0.5476
20	1.7580	2.1740	4.7263
25	1.6680	2.0840	4.3431
30	1.0620	1.4780	2.1845
Average FD	-0.4160	$\sum (F\boldsymbol{D} - \textbf{Average } \boldsymbol{FD})\textbf{2}$	27.8464

Hence, Std Dev (FD) = 2.1543

$$\Delta FD=\sqrt{(2 * 2.1543)2 + 0.12}=4.3098$$

Hence, ΔFD is calculated to be 4.3098 N for 30 m/s. Uncertainty Analysis on CD The uncertainty in the coefficient of drag was calculated using Equation 18 bow:

$\Delta CD = \sqrt{}$ (ΔFD 2) FD+ $(-2\Delta V)^2$

Where ΔFD for 30 m/s = 4.3098 N and 20 m/s = 1.3563 N and ΔV = 0.022876 m/s is obtained based on the calculation above.

Table 13: Coefficient of Drag uncertainty calculation for 20 m/s.

The angle of Attack	F_D	ΔC_D

Table 14: Coefficient of Drag uncertainty calculation for 30 m/s.

(°)		
0	-0.4900	2.7683
5	-1.3740	0.9882

10	-1.4980	0.9066
15	0.0940	14.4286
20	-1.6720	0.8125
25	-1.2680	1.0706
30	-0.3660	3.7060
Average ΔC***D***		3.5258

Hence, the average value on ΔCD for 20 m/s is calculated to be 3.5258.

Hence, the average value on ΔCD for 30 m/s is calculated to be 4.9651.

The angle of Attack (°)	F_D	ΔC_D
0	-3.2300	1.3351
5	-3.0900	1.3955
10	-1.4040	3.0700
15	0.3240	13.3019
20	1.7580	2.4520
25	1.6680	2.5842
30	1.0620	4.0584
Average ΔC***D***		4.9651

6. Result And Discussion

6.1 Error Analysis on Wind Tunnel Calibration

From the comparison data in Table 1 and Table 2, we can determine the accuracy of the wind tunnel by doing the calculation on a root mean square error (RMSE) to characterize the wind tunnel accuracy. The formula for RMSE is as below:

$$RMSE = \sqrt{\sum_{n}^{n=1} \frac{\left(V_{n_{manual}} - V_{n_{Pitot\ Tube}}\right)^2}{n}} \quad (16)$$

Where Vmanual is the velocity given by the manufacturing manual and VPitot Tube is the velocity determined by using Pitot Tube during the calibration process. To calculate RMSE, we square each error (the deviation from both readings), then calculate the arithmetic average of those values, and finally, take the square root of the average. All the data tabulate were recorded in Table 6 as below. From this calculation, hence we can see the RMSE for this wind tunnel is approximately 3.92%. One of the factors contributing to the error of the experiment is the irregular wind flow because the air is not uniformly distributed along the wind tunnel. The axial fan generating the wind may rotate at an uneven frequency due to blade angle and shaft lubrication. Surface roughness over multiple usages of the NACA 0015 airfoil causes differential flow over the surface which in turn causes error. On top of that, an assumption of constant temperature is used for this experiment while in reality, the fluctuation of temperature in the wind tunnel will impact the error readings produced.

Table 15: Root Mean Square Error Table.

Frequency, Hz	V, m/s		Error	Error^2
	Manual	Pitot Tube	(Manual - Pitot Tube)	
5	5.2	4.07	1.132	1.28
6	6.5	4.98	1.518	2.30
7	7.4	5.75	1.647	2.71
8	8.4	7.05	1.354	1.83
9	9.5	8.14	1.364	1.86
10	10.6	9.10	1.504	2.26
15	15.4	15.75	-0.355	0.13

20	20.5	21.91	-1.406	1.98
25	25.5	29.05	-3.550	12.60
30	30.5	35.46	-4.962	24.63
35	35.5	41.48	-5.984	35.81
40	40.5	47.61	-7.113	50.59
45	45.5	53.35	-7.849	61.61
Root Mean Square Error (RMSE)				3.92

6.2 Experiment

The calculation for Reynold Number (Pitot Tube).

V=Velocity (m/s)

L=Chord Length(m)

V=Kinematic viscosity (m2/s

Since the experiment was conducted at 25C, hence the kinematic viscosity value is constant at 0.00001552 m2/s.

Reynold Number at 20 m/s= $\frac{(20)(0.14)}{0.00001552}$ = 18040

Reynold Number at 30m/s = ((30) (0.14))/0.00001552=270619.

The Reynolds number when the air velocity is set at 30 m/s is higher than when the air velocity is set at 20 m/s. From above, both the value is below 1 × 10 5 for the Reynolds number thus the inertial forces do not dominate viscous forces and the flow is therefore not turbulent.

Figure 6 demonstrates the trends of the lift force of aerofoil are greater when higher velocity (30 m/s) instead of low velocity (20 m/s). This is mainly due to high velocity creating a displacement (loss of flow area) as air flows around the aerofoil according to the continuity law. Theoretically, according to the Bernoulli Equation, the high velocity decrease the pressure on top of the aerofoil. Thus, led to a positive direction of lift due to the greater loss of pressure on top of the aerofoil rather than the bottom part which is seen in Figure 7. In addition, the frictional force is created from the larger drag force. Thus, the low drag force is necessary to increase the efficiency of aircraft. On the other hand, the increase of the lift force is influenced by the angle of attack. As the angle of attack increases, the lift force increase. Theoretically, laminar flow at the trailing edge of aerofoil occurs at a small angle of attack. However, the possibility of the aerofoil to expose to the wind is higher when there is a large angle of attack. This is mainly due to the top surface of the aerofoil experiencing low displacement when at low velocity. This led the turbulence to have occurred from the laminar flow which is known as the separation point. It is anticipated that flipping over the NACA 0015 will not affect its performance. This is mainly due to the symmetric shape of an aerofoil in the present experiment. Unless the shape of the aerofoil (non-symmetric) might change the behavior of the lift and drag force of the aerofoil.

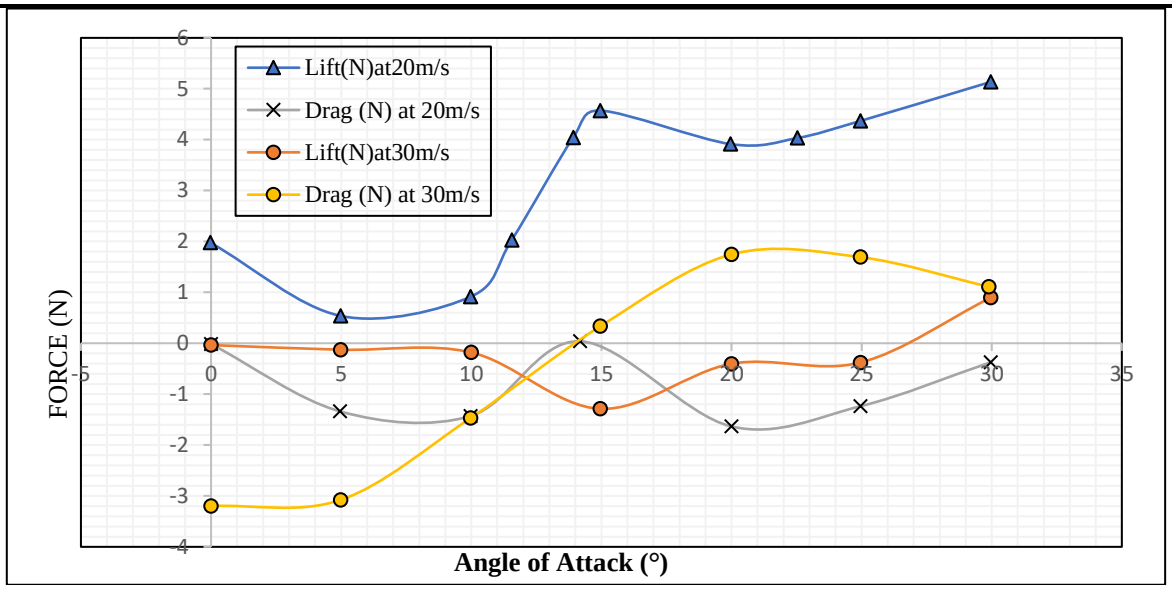

Figure 6. Lift Force and Drag Force against AoA Gra

Based on Figure 7, it is shown that the coefficient of lift increases as the angle of attack increases. In terms of the value of the coefficient lift of 20 m/s is higher than 30 m/s. It is also seen that the Drag Coefficient for 30 m/s is higher compared to 20 m/s when at a fixed angle. At 30 m/s, the drag force might increase as the angle of attack increases and produce a low coefficient of lift as compared to the speed of 20 m/s. It is noted that during the high speed of 30 m/s, the aerofoil cannot distribute the wind properly due to a chaotic flow pattern after the increment of the angle of attack. By referring to the coefficient of lift for a wind speed of 30 m/s, it increases in the same pattern as the coefficient of lift of 20 m/s but on a small scale lower. The gap between the drag coefficient and the lift coefficient for a wind speed of 20 m/s is bigger than the gap between the coefficient of lift and drag for a wind speed of 30 m/s. This behavior could be caused by the influence of speed which can shrink the level of drag force and the drag force.

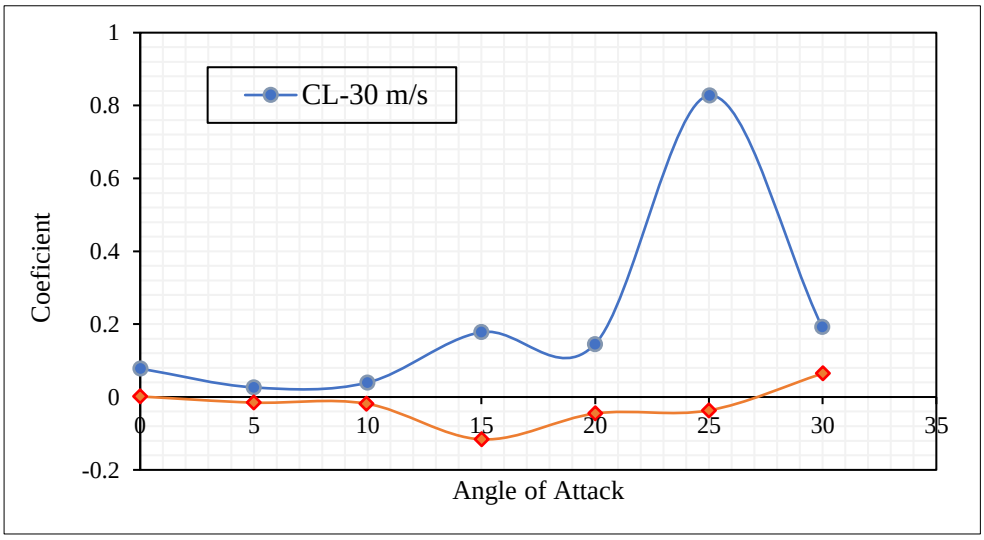

Figure 7. Coefficient of Lift (CL) Vs AoA.

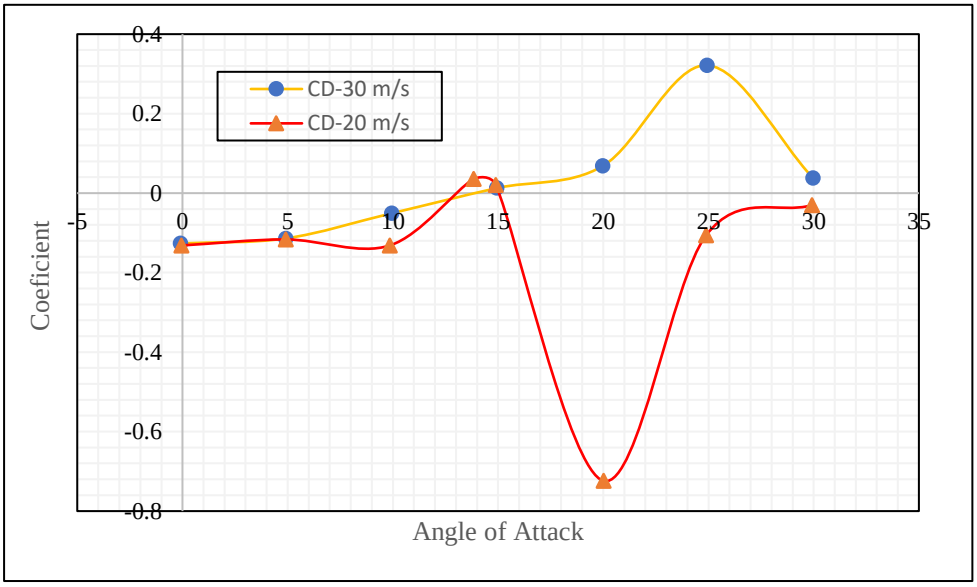

Figure 8. Coefficient of Drag (CD) Vs AoA.

Based on figure 8, shows that both the coefficient for 20 m/s and m/s is not the same as the angle of attack varies. Because lift and drag are both aerodynamic forces, the ratio of lift to drag means the efficiency of the aerofoil itself. Comparatively between the speed of 30m/s and 20m/s, the ratio of lift to drag for speed 20 m/s is higher than the speed of 30 m/s. The reason can be explained by the high efficiency of aerofoil by high lift force with low drag force at a speed of 20 m/s. The low drag force can reduce the formation of turbulent flow, therefore, can produce a high lift force. In addition to that, it can be seen that the ratio coefficient is much more stable for 20 m/s which may be because it is less turbulent compared to higher speeds. The result of the ratio for a wind speed of 30 m/s also produced irregularity between the coefficient of drag which may have been caused by the high thrust needed to sustain the flow pattern of wind on the boundary layer of aerofoil because of high speed. A different angle of attack on the wind flow for a speed of 20 m/s could produce a stable ratio whereas for a speed of 30m/s, the fluctuation has happened and this is due to the coefficient of drag which is produced unstable.

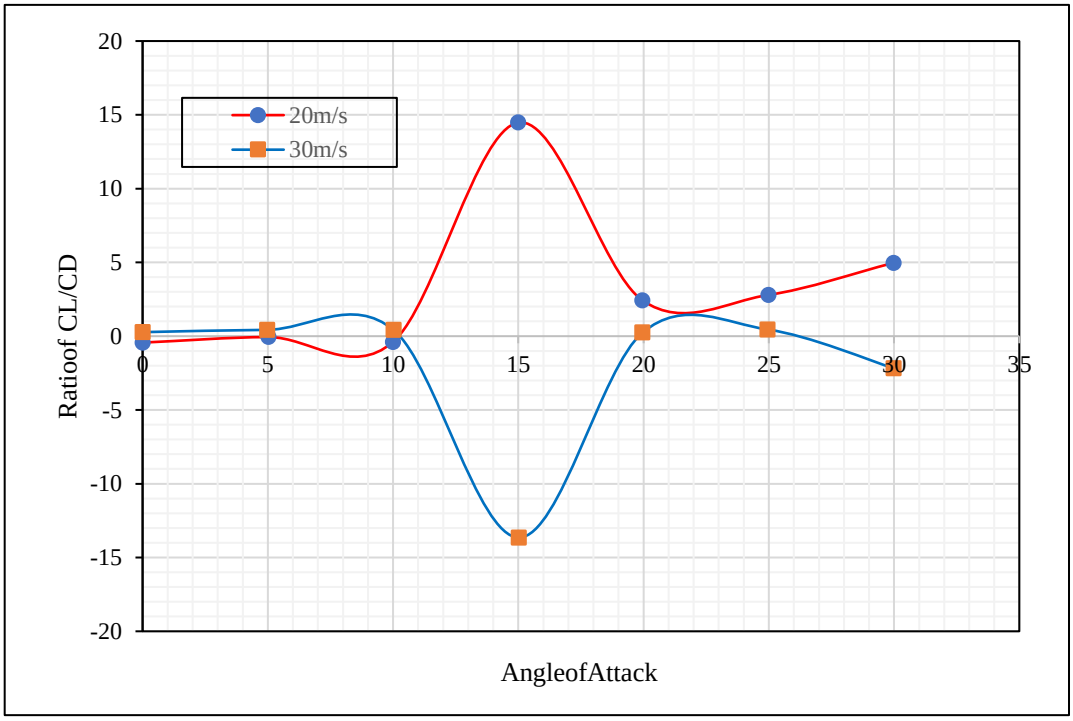

Figure 9. The ratio of the coefficient of Lift and Drag (CL/CD) vs AoA.

6.3 Flow Visualization Using Tuft

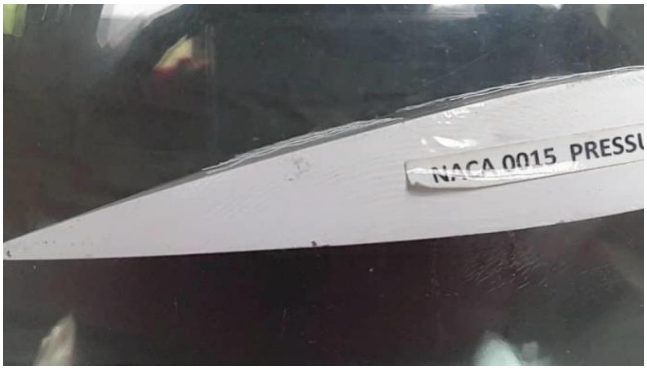

Figure 10: Flow visualization at air velocity 2 m/s AoA 0°

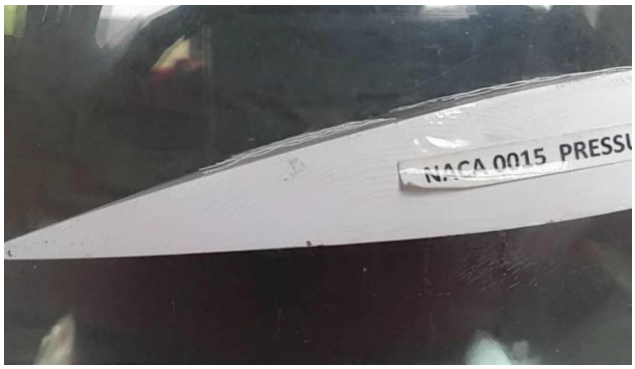

Figure 11: Flow visualization at air velocity 2 m/s AoA 5°

Figure 12: Flow visualization at air velocity 2 m, AoA 10

Figure 13: Flow visualization at air velocity 2 m, AoA 15°

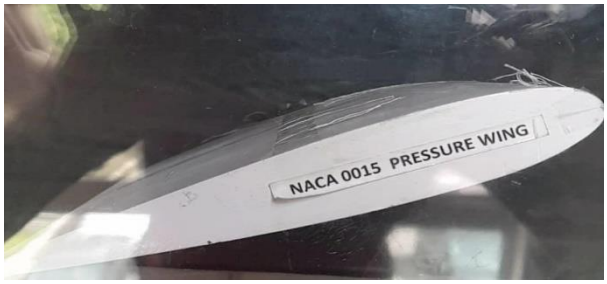

Figure 14: Flow visualization at air velocity 2 m/s AoA 20°

Figure 15: Flow visualization at air velocity 2 m/s AoA 25°

Figure 16: Flow visualization at air velocity 2 m/s AoA 30°

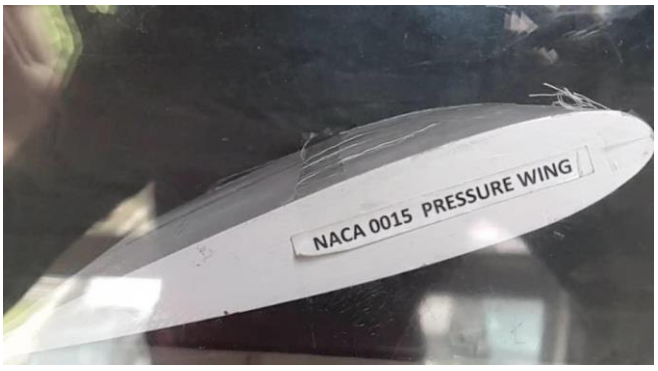

Figure 17: Flow visualization at air velocity 3 m/s AoA 0°

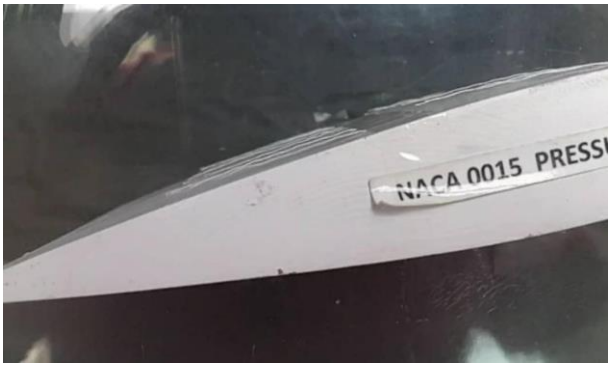

Figure 18: Flow visualization at air velocity 3 m/s AoA 5°

Figure 19: Flow visualization at air velocity 3 m/s AoA 10°

Figure 20: Flow visualization at air velocity 3 m/s AoA 15°

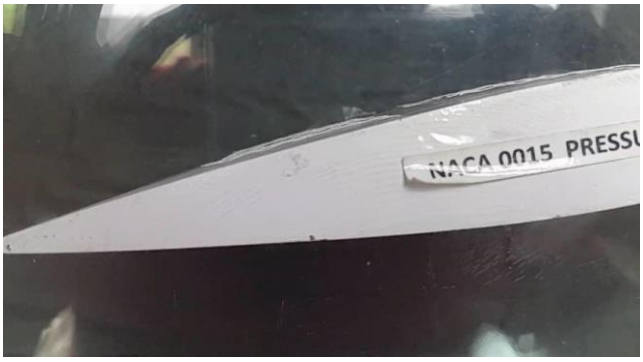

Figure 21: Flow visualization at air velocity 3 m/s AoA 20°

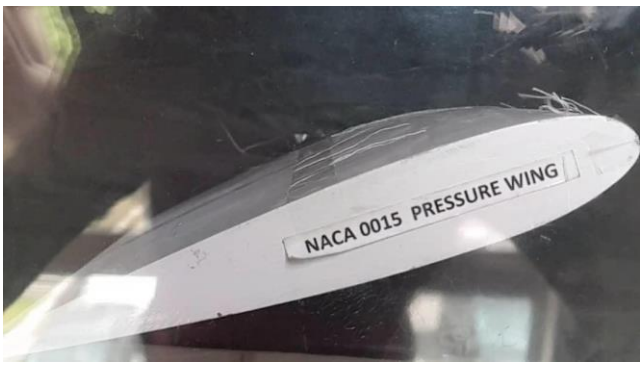

Figure 22: Flow visualization at air velocity 3 m/s AoA 25°

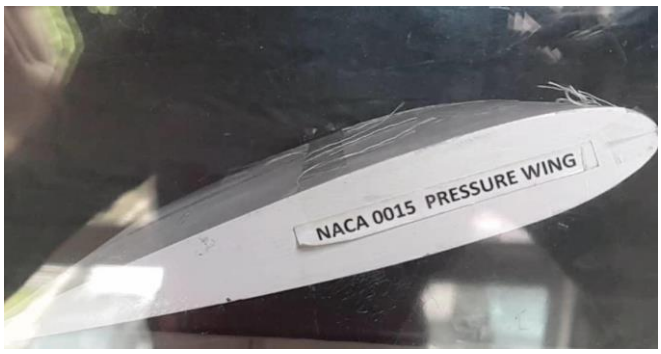

Figure 23: Flow visualization at air velocity 3 m/s AoA 30°

From Figure 10 to Figure 23 To attach tufts to a model's surface, one can use adhesive like tape or glue. These tufts are then blown downstream by the air flowing over the model. If the entire model is covered in tufts, any areas of strong cross-flow, reverse flow, or flow separation will be indicated by the direction of the tufts. Additionally, tufts can reveal regions of unsteady flow when captured on film or video. As in Figures 10 to 14 and Figures 17 to 19, the image shows the thread moving in one direction due to the steady state condition. In Figures 10-11 and

Figure 20- 23, the vortex produced will cause the tuft to move vigorously and in the opposite direction due to wake. The pressure there decreased and the pressure drag on the body subsequently rose as a result of the energy lost by the very turbulent motion in the wake, despite the predicted Reynolds Number showing that it is somewhere along the transition phase from laminar to turbulent. The size of the wake, which in turn depends on the position of separation, greatly influences the pressure drag's intensity. When the body is shaped such that separation only occurs well in the rear and the wake is small, the pressure drag is also small. A streamlined body is one with such a shape.

Both turbulent and laminar boundary layers can separate. Laminar boundary layers, however, are significantly more likely to split apart than turbulent ones. This is so that the slow-moving fluid close to the surface can be stopped more easily by the unfavorable pressure gradient because, in a laminar boundary layer, the rise in velocity with distance from the surface is less rapid. The boundary layer can endure an unfavorable pressure gradient for a while before separating for flow characteristics above which are turbulent.

Flow separation happens when the boundary layer moves against an unfavorable pressure gradient, causing the velocity of the boundary layer about the object to decrease significantly. This detachment of fluid flow from the object's surface results in the formation of eddies and vortices. Boundary layer separation refers to the broader wake created when the boundary layer separates from the surface. This occurs when the part of the boundary layer closest to the wall or leading-edge experiences a reversal in the flow direction. The point where the forward and backward flow meet, and the shear stress is zero, is known as the separation point. At this point, the entire boundary layer thickens abruptly before being pushed away from the surface by the reversed flow at its bottom.

7. Conclusion

From the experiment, the NACA 0015 experiences stalling in the range of. $20° < \alpha \leq 30°$ AOA which is at 25° when the speed is set at 30 m/s while when set at 20 m/s, the stalling occurs at 15° which lies between $10° < \alpha < 20°$. Flow separation is caused by the stalling phenomena. The performance of the NACA 0015 is expected to be the same despite it being flipped over. This is mainly due to the symmetric shape of an aerofoil in the present experiment. Unless the shape of the aerofoil (non-symmetric) might change the behavior of the lift and drag force of the aerofoil. The proposed instrumentation system is acceptable with several conditions. The instrumentation system used here for this experiment should be calibrated accordingly as varying usage between high and low Reynolds number tend to reduce the actual time for the next calibration date while lab types of equipment tend to be calibrated based on dates given by the supplier. Other recommendations include the fan blade balancing and the lubrication for the fan should be intact to produce an even flow for the instruments to provide accurate and precise reading.

References

1. Ravikumar T.; Prakash, S.B. Aerodynamic analysis of supercritical NACA SC (2)-0714 airfoils using CFD. Int. J. Adv. Tech. Eng. Sci. 2014, 02, Issue 07, 285-293.
2. Mccroskey, W. J.; Kutler, P.; Bridgeman, J. O.; Status and prospects of computational fluid dynamics for unsteady transonic viscous flows. NASA_NTRS_Archive_19850003729.
3. Siva, V. Analysis of ground effect on a symmetrical airfoil. Int. J. Eng. Res. App.
4. 2015, 5, Issue 10, (Part - 2),40-42.
5. Zerihan, J.; Zhang, X. Aerodynamics of a single element wing in ground effect, J. Aircr. 2000, 37, No. 6,1058-1064. DOI: 10.2514/2.2711.
6. Carr, L.W.; Mcalister, K.W.; Mccroskey, W.J. Analysis of the development of dynamic stall based on oscillating airfoil experiments, NASA TN D-8382, Ames Research Center and U.S. Army Air Mobility R&D Laboratory Moffett Field, Calif. 94035. Available online:

https://ntrs.nasa.gov/search.jsp?R=19770010056 (accessed on 13.04.2019)
7. "A Description of the NACA 4-Digit System" Available online: http://www.akiti.ca/NACA4Bkgrnd.html(accessed on 13.04.2019)
8. http://plastrochem.com/hydro_4_a8.html.